1.1.2 Remote sensing of marine litter and debris with spaceborne bistatic radar

by Chris Ruf, Madeline Evans, Yulin Pan, Yukun Sun, University of Michigan

1.1.2.1 Overview

The remote detection of microplastics using spaceborne radar relies on measuring the effects that surfactants and other ocean constituents have on the ocean surface properties measured by spaceborne bistatic radars. Many of these constituents tend to have similar transport mechanisms as the microplastics and tend to accumulate in the same ocean convergence zones. Surfactants are detectable from space because of the weakened responsiveness of the ocean surface to wind-forced roughening that results when they are present. The first application of this remote sensing method was demonstrated using observations by the NASA Cyclone Global Navigation Satellite System (CYGNSS), a constellation of eight satellites in Low Earth Orbit [Evans and Ruf, 2021]. Each satellite acts as the receiver end of a bistatic radar system, wherein signals are transmitted by GPS satellites and reflected off of the ocean surface. CYGNSS uses these reflected GPS signals to produce Delay Doppler Maps (DDMs), utilized primarily to measure wind speed close to the ocean surface [Ruf et al., 2016]. CYGNSS is directly sensitive to a statistical measure of ocean surface roughness, the mean-square slope (MSS). Microplastics are detected indirectly via anomalies in the MSS from their expected value for a given wind speed. MSS anomaly measurements are averaged over a one-year time window in 1^ox1^o lat/lon grid cells, representing the annual distribution of roughness suppression. These annual average values are matched up geographically with global distributions of microplastic concentrations estimated by ocean circulation models [van Sebille et al., 2015]. This results in an empirical relationship between microplastic concentration and roughness suppression. Subsequently, this method can be used to detect microplastic transport globally on shorter timescales, revealing seasonal patterns and outflow events from major rivers.

1.1.2.2 Description of Data Processing

Description of CYGNSS Satellite Data

One year of CYGNSS Level 2, Version 2.1 MSS measurements (time-tagged, 25 km resolution) are matched up to GDAS Blended Sea Winds (6-hour, 0.25^o resolution) using a linear interpolation in time of the GDAS winds that are closest in location to CYGNSS. Matchup winds are defined as the vector sum $\sqrt{u^2 + v^2}$ of GDAS 10-meter reference wind vector components, (u, v). One year of data within 1 Jun 2017 – 31 May 2018 are used here, excluding low quality data, specifically, data affected by satellite calibration and file reader errors (13-17 April 2018 and 5 January 2018, respectively) and flagged data specified by the Fully Developed Seas wind speed product flag.

Description of Microplastic Model Data

Three global models of buoyant plastic debris from [van Sebille et al., 2015] are used to calibrate the microplastic concentration retrieval algorithm. The models estimate a steady state global distribution of marine debris and vary by microplastic source, sink, and transport functions.

The van Sebille model originates plastic along coastlines, scaling input by human population within 200 km of the coastline and by the amount of mismanaged waste per country. This model does not include sinks. Plastic transport is determined by particle travel probabilities calculated from a historical global set

of satellite tracked drifter buoys from the NOAA Global Drifter Program. Results of microplastic concentrations determined by the global distribution of plastics after a 50-year model run.

The Lebreton model designates the source of plastic as major river mouths, along coastlines, and on major shipping routes. Plastic input varies spatially with levels of human population and urban development and temporally based on global plastic production data. Ocean velocity fields from the HYCOM global circulation model determine plastic movement, excluding sinks. The model estimates global microplastic distribution after a 30-year run time.

The Maximenko model originates plastic uniformly over the global ocean. As in the van Sebille model, the transport algorithm is based on drifter buoy data from the NOAA Global Drifter Program. The Maximenko model does include a sink and allows plastic particles to exit the system when they enter its coastal grid cells. Global microplastic distribution is modelled after a 10-year run time.

Description of MSS Anomaly Algorithm

MSS anomalies are used to measure of deviation of measured ocean surface roughness from the expected roughness, given the actual wind speed above the ocean surface. The expected roughness is determined by the empirical relationship between collocated wind speed and MSS in regions of low plastic concentration. GDAS wind speed and CYGNSS MSS measurements from 1 Jun 2017 – 31 May 2018 located within two control regions ([10º-25ºS, 105º-120ºE] and [10º-20ºN, 128º-143ºE]) determine the following empirical relationship:

$$MSS_{mod} = \begin{cases} 0.0035(U + 0.62) & if\ U \leq 3.49\ m/s \\ 0.0035(6\ln(U) - 3.39) & if\ U > 3.49\ m/s \end{cases} \quad (1)$$

MSS anomalies are normalized with respect to the modelled MSS:

$$MSS_{anom} = \frac{MSS_{obs} - MSS_{mod}}{MSS_{mod}} \quad (2)$$

MSS anomaly measurements collocated with wind speeds of 3-11 m/s are used for further analysis to determine the relationship between ocean surface roughness suppression and microplastic concentration.

Description of Microplastic Retrieval Algorithm

A map of average MSS anomalies over one year with 1-degree resolution is used to tune a retrieval algorithm to calibrate the long-term relationship between ocean surface roughness suppression and microplastic concentrations. Three global models of microplastic concentration from van Sebille, et al., 2015 were used in this step. These models offer static predictions of microplastic concentration globally with consistent spatial 1-degree resolution. Differences in these predictions exists as a result of varying particle source, sink, and transport functions, as well as varying model run-times.

Within a central range of data, spatially-matched annual average MSS anomalies and static microplastic concentrations from the van Sebille model are used to train a log-linear relationship:

$$\rho = 2035\exp(-23.18 MSS_{anom}) \quad (3)$$

where ρ represents microplastic number density (#/km^2). Negative MSS anomalies correspond to increased wave damping and higher microplastic concentrations. This equation is utilized in the microplastic retrieval

algorithm. Spatiotemporally close measurements of microplastic concentration are geometrically averaged to provide global maps of microplastic concentration on varying time scales.

1.1.2.3 Results

Temporal variability of ocean plastic debris on a global scale remains unresolved by sparse net trawl sampling, steady-state models, and localized remote sensing methods. Continuous spaceborne radar observations are able to resolve temporal variations in the global microplastic concentration on seasonal timescales and in more localized regions on shorter timescales. Monthly maps of global microplastic concentration derived from CYGNSS observations (Fig 1) indicate a strong seasonal dependence of the concentration in the major Pacific and Atlantic Ocean gyres.

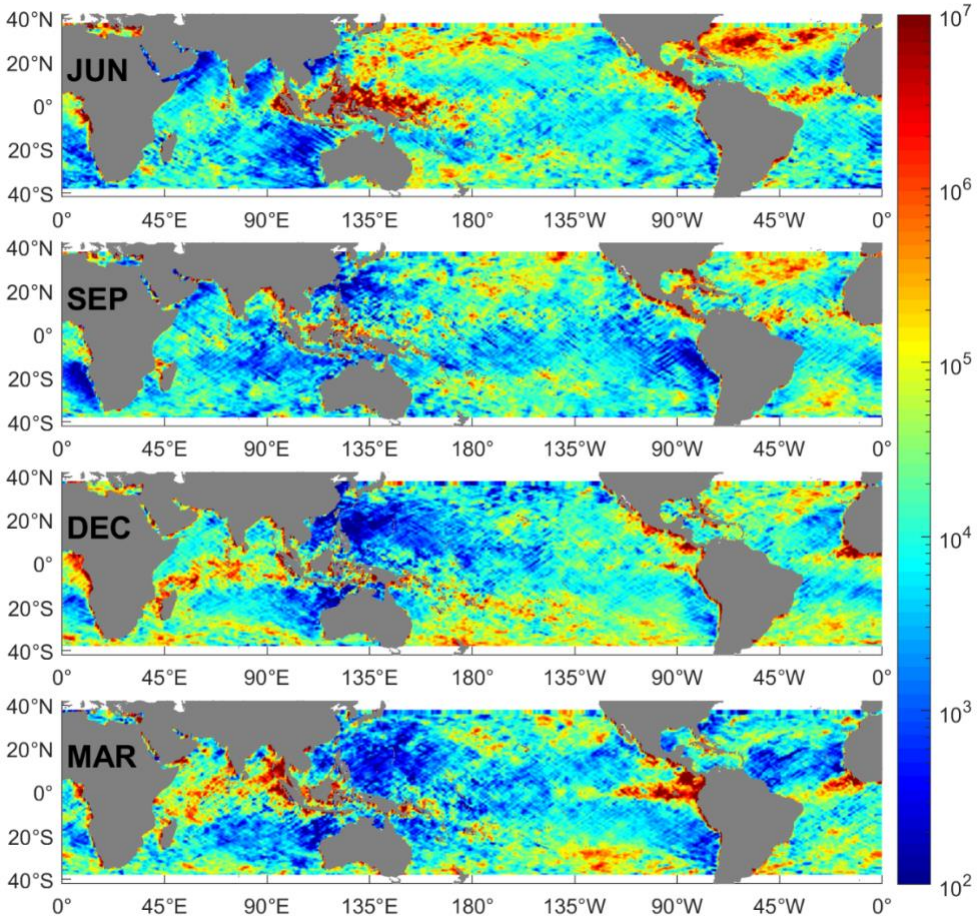

Fig. 1. One-month averages of microplastic number density concentration (#/km^2, $\log_{10}$ scale) derived from CYGNSS spaceborne radar observations in Jun-Sep-Dec 2017 and Mar 2018. Higher microplastic concentrations are observed during the austral and boreal summer in both the Atlantic and Pacific basins.

The monthly maps in Fig. 1 indicate higher microplastic concentrations in both the Northern and Southern Hemisphere during summer months, and lower in the winter. There are several possible explanations. Lower concentrations in winter may be a result of the increase in vertical mixing of near-surface ocean

layers that is commonplace in winter months. Higher concentrations in summer could be due to greater biological activity, e.g. involving phyto- and zoo-plankton or other marine biota, during the summer months. There is some indication of a similar seasonal dependence in the limited ground-truth (i.e. net trawl) data available from the 1970s to the present. However, these data tend to have a large seasonally-dependent sampling bias due to the relative difficulty of sample collection during cold weather months.

The finding of a strong seasonal dependence in the spaceborne radar observations suggests several follow on recommendations. An expanded campaign of in situ microplastic sampling is recommended within the major ocean gyres which covers the full annual cycle of seasonal variations. The existing ocean circulation models of microplastic distribution are steady state solutions without any temporal dependence. It is recommended that consideration be given to expanding these models by incorporating appropriate seasonal dependencies into their relevant oceanographic features so that seasonal changes in microplastic concentration can be resolved. These efforts would help to validate the spaceborne radar observations. They and the radar measurements might also be used to optimize clean-up efforts and to improve our understanding of microplastic transport mechanisms.

CYGNSS observations can also be narrowed to more localized areas and on shorter time scales. One example focuses on potential sources of ocean microplastic at the mouths of the Yangtze, Qiantang and Ganges Rivers. These rivers are likely large contributors of microplastics to the global oceans due to the abundance of mismanaged waste present in their river basins. Microplastic concentrations in the East China Sea are shown in Fig. 2 averaged over four different time periods. The annual average in Fig. 2(A) has no discernable outflow from the Yangtze or Qiantang Rivers. However, the three particular weekly averages shown in Figs. 2(B-C) reveal outflow plumes emanating from the mouths of the two rivers. These results suggest that the outflow is occurring irregularly in episodic bursts.

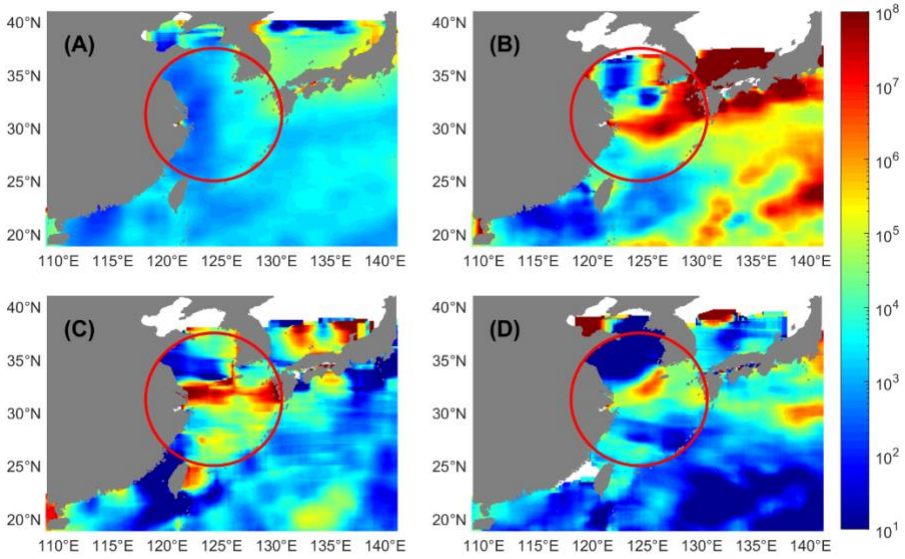

Fig. 2. Estimated microplastic number density concentration (#/km^2, $\log_{10}$ scale) outflow into the East China Sea. (A) The annual average of microplastic concentration. (B-D) One-week averages of high concentrations of microplastics emerging from the Yangtze and Qiantang River mouths and dispersing into the East China Sea in the region highlighted by red circles. One-week averages shown are during (B) 22–28 Jun 2017, (C) 27 Oct – 2 Nov 2017, and (D) 2–8 Dec 2017.

As with the global scale seasonal results, this localized behavior in near-coastal regions can also be influenced by other factors which may contribute to the suppression of wind-driven roughening of the ocean surface. Near-coastal regions often contain higher concentrations of non-plastic and surfactant contaminants such as algal blooms caused by agricultural runoff, jetsam and flotsam from sea vessels, and other floating organic material such as sea foam or wood. Additionally, the effect from river currents themselves can introduce perturbations to the the sea surface roughness. All of these factors can also affect the roughness anomaly measurements used to estimate microplastic concentration and so should be considered complicating ancillary dependencies. Further investigations into these effects are recommended.

1.1.2.4 Wave Tank Experiment

1.1.2.4.1 Overview

Through wave tank experiments, we study the mechanism associated with the mean square slope (MSS) roughness anomalies detected by CYGNSS as well as the general physics of wave damping by floating particles and surfactants. In the experiments, waves are generated either by a mechanical wave maker or by fan-generated wind. The resulting MSS of the water surface is compared for clean water and water with additives. For floating particles, we use two sizes of particles with diameters 0.5 cm and 0.8 cm (both in the range of oceanic microplastics) and consider their partial coverage of the surface with varying area fraction. For surfactants, we use a soluble surfactant Triton X-100 (which has been commonly used in many previous studies) with different concentrations. Within the scope of remote sensing applications (e.g., CYGNSS), we find that the effect of floating particles on MSS (with CYGNSS cut-off wavenumber) is negligible even at area fractions much larger than that in real oceanic situations. The mechanically generated waves with surfactants of the highest concentration in the test results in a $O(10\%)$ reduction relative to the MSS in clean water. Furthermore, the wind-waves generated with moderate surfactant concentration leads to a $O(17\%)$ reduction from the MSS in clean water, for a wind speed about 9 m/s. Considering the MSS anomalies observed by CYGNSS, which corresponds to CYGNSS MSS $O(20\%)$ lower than the results from the calibrated Katzberg model [Katzberg et al., 2006], we conclude that the effect of surfactants in a wind sea is the most influential factor for this remote sensing application. A systematic presentation of this work can be found in [Sun et al. 2021].

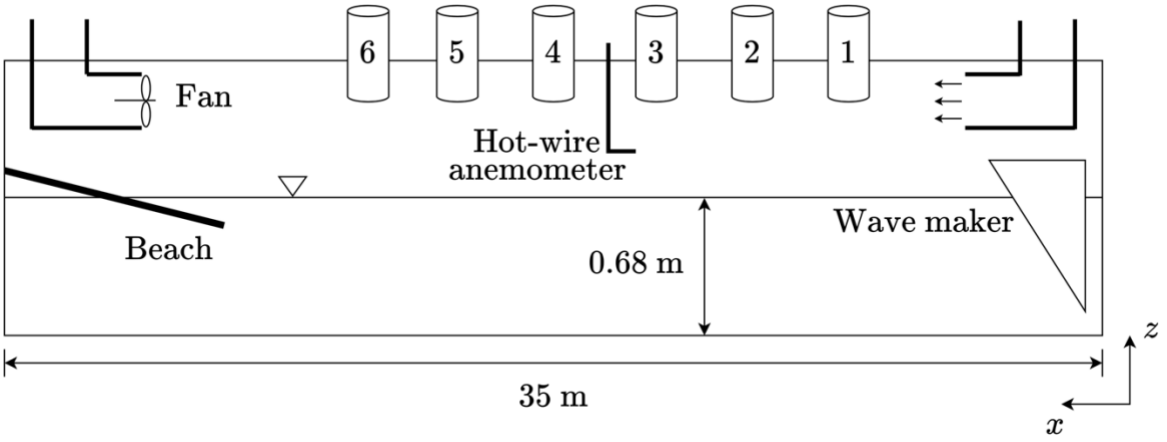

Fig. 3. Schematic sketch of the side view of the wave tank, including a wave maker, a wind tunnel, six ultrasonic sensors, a hot-wire anemometer, and a beach. The spacings between the sensors are not perfectly scaled.

1.1.2.4.2 Description

Description of the Facility and Input Parameters

The experiments are conducted in the wind-wave tank facility (Fig. 3) in the Marine Hydrodynamics Laboratory (MHL) at the University of Michigan. The tank is 35 m long and 0.7 m wide with a water depth of 0.68 m. Waves can be generated by either a mechanical wave maker or wind through an open-loop tunnel, and are dissipated at one end of the tank by a beach with slope of 5°. The wavemaker is wedge-shaped, with its motion numerically actuated by a feedback-controlled servo motor with a proportional-integral-derivative (PID) controller, according to an input frequency spectrum. A two-parameter wind-wave spectrum empirically developed for fully developed seas is used in this study. Winds are generated by a 40-hp fan in the wind tunnel, producing three wind speeds of 4.29, 6.59, and 9.09 m/s in this study. Surface elevations are measured by 6 ultrasonic sensors mounted on top of the wave tank, with a sampling frequency fixed at 100 Hz.

Description of the Testing Procedures

For experiments with microplastics, we use two types of particles both made of polypropylene: one as microbeads with irregular shape and average diameter $D_p \approx 0.5$ cm, and the other as plastic balls with regular shape and diameter $D_p \approx 0.8$ cm. For technical simplicity, we focus on mechanically generated waves in this part. In each experiment, we first place the particles in the wave tank at 8.53 m from the wave maker in calm water. The particles then spread out both up- and downstream due to particle-particle and particle-surface interactions until a balance is reached with a recorded length of L_i. As waves pass through the particles, they further spread out and drift downstream with the final spreading length (after waves pass through) recorded as L_f. The concentration of particles with varying spreading length can be quantified by defining an (average) area fraction

$$C = \frac{N_p S_p}{W\overline{L}} \tag{4}$$

where N_p is the number of particles, $S_p = \pi D_p^2/4$ is the planform area of one particle, W is the width of the tank and $\overline{L} = (L_i + L_f)/2$ is the average spreading length. In practice, we choose N_p such that the value of C ranges from 0.1% to 20%, with the lowest fraction close to oceanic microplastics concentration. Due to the drift of particles, the final length L_f may cover the surface area beneath sensors 1 and 2. In order to robustly measure the effect of particles on waves (i.e., to avoid the acoustic reflection from particles and consistently consider waves after passing through all particles), we focus on sensor measurements downstream of the particle patch L_f. In addition, we exclude data from sensor 6 since it is relatively far away from the particles (so that the wave properties may be modified too much by nonlinear interactions instead of particle damping). Therefore, we investigate the results based on sensors 3, 4, and 5 for floating particle experiments. A total of 9 values of C in this range are tested (5 and 4 for smaller and larger particles), with each experiment repeated for 3 times to quantify the uncertainty level.

Symbol	Γ_0	Γ_1	Γ_2	Γ_3	Γ_4	Γ_5	Γ_6	Γ_7	Γ_8

$\Gamma \times 10^5$ (mol/L)	0	0.05	0.20	0.31	0.61	0.81	1.51	3.11	5.09
σ (mN/m)	72.0	69.1	60.1	57.5	54.4	53.5	49.9	45.5	43.5

Table 1. Surfactant concentrations $\Gamma_0 \sim \Gamma_8$ used in the experiments, with the corresponding values of surface tension σ.

For surfactants, we consider using Triton X-100 with nine concentrations $\Gamma = \Gamma_0 \sim \Gamma_8$ (in terms of mol/L) as listed in Table 1, with Γ_0, Γ_1, Γ_2, Γ_6, Γ_7, and Γ_8 tested for mechanically generated waves, and $\Gamma_0 \sim \Gamma_7$ tested for wind waves. The surface tension σ for each concentration is measured from water samples a surface tensiometer, which uses the Wilhelmy plate method based on the balancing of surface tension, gravitational, and buoyant forces on a platinum plate [e.g. Lapham et al., 1999]. The measured surface tensions are listed in Table 2, all of which are below the critical micelle concentration (CMC) limit for Triton X-100, which is $\Gamma = 23 \times 10^{-5}$ mol/L corresponding to a saturated surface tension $\sigma = 30.6$ mN/m. In each day, we perform a total of (maximum) 12 experiments related to one concentration Γ, that include three cases with different wind speeds and one case with the wave maker, with each repeated for three times. At the end of each day more surfactants are added to the tank until the next level of desired concentration Γ is reached. A circulation pump is turned on overnight to well mix the surfactant and water before the starting of experiments on the next day.

Description of Physical Quantities of interest

Frequency spectra of surface elevations are calculated from the time series measured by the sensors in a time interval of 100 s of stationary state (in time). We compute the spectra as an ensemble average over spectra of 9 segments of the time series with 50% overlapping of each two segments. For each segment $\Delta t = 20$ s with 2000 data points, we use a Tukey window function to taper the tails of the segment and evaluate the spectrum as

$$S_f(f) = \left(\frac{\Delta t}{2}\right) |\hat{\eta}(f)|^2 \tag{5}$$

where $\hat{\eta}(f)$ is the coefficient of cosine Fourier series of the tapered segment. Given $S_f(f)$, the MSS is defined as

$$\text{MSS} = \int_0^{k_c} k^2 S(k) dk \tag{6}$$

where k is the wavenumber, $S(k) = gS_f(f)/(8\pi^2 f)$ is the omni-directional spectrum, and k_c is the cut-off wavenumber depending on the incident angle and carrier wavelength in the measurements by CYGNSS with an average value of 7.5 rad/m [Wang et al., 2020]. As defined, MSS $\rightarrow \overline{\nabla\eta \cdot \nabla\eta}$ (variance of surface elevation gradient) for $k_c \rightarrow \infty$, and otherwise MSS quantifies the surface roughness up to a finite scale k_c.

1.1.2.4.2 Results

While many results are produced in this set of experiments (presented systematically in [Sun et al. 2021]), we only briefly summarize the findings and then focus on those that are most relevant to the CYGNSS application in this report. For experiments with floating particles, we find that the damping effect by particles on surface waves critically depends on the area fraction of coverage, irrespective of the sizes. Damping effects on both energy and MSS (with $k_c = 1000$ rad/m) are only observed for fractions above $O(5-10\%)$, which are much higher than the oceanic microplastics situation of $O(0.1\%)$. For surfactants, experiments with mechanically generated waves show that they generally result in enhanced damping for both the energy and MSS (even at CYGNSS cut-off wavenumber). In the experiments of waves generated

by wind, we find that the presence of surfactants significantly suppresses the wave generation, due to its combined effect of reducing the wind stress and increasing the surfactant-induced damping. The wind stress, obtained from the measured wind profile, is further found to follow an exponential dependence on the surface tension, and a power-law dependence on the concentration level of the surfactant (with the power-law exponent linearly related to the wind speed).

When considering the CYGNSS cut-off wavenumber $k_c = 7.5$ rad/m, Fig. 4 shows a typical result of MSS as a function of k_c measured by sensor 3 for both sizes of particles at their highest area fraction C, along with the reference results in clean water. It is clear from the plots that for $k_c = 7.5$ rad/m, the effect of particles on MSS is negligible even for the highest concentration (let alone the oceanic concentration which is much lower). Therefore, the results are sufficient for us to conclude that the MSS anomalies observed by CYGNSS are not caused by the effects of microplastics as floating particles.

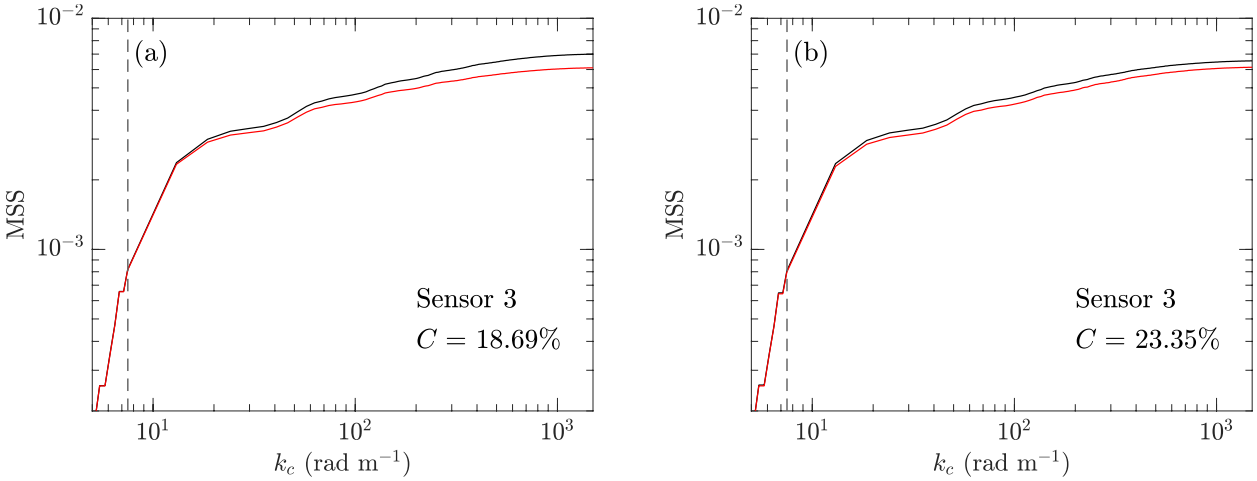

Fig. 4. MSS computed with different k_c with (a) particles of $D_p \approx 0.5$ cm, $C = 18.69\%$ (red line) and (b) particles of $D_p = 0.8$ cm, $C = 23.35\%$ (red line). The reference clean-water results (black line), as well as the indication of $k_c = 7.5$ rad/m (dashed line), are shown in both (a) and (b).

Fig. 5(a) shows the MSS at sensor 6 as a function of k_c for mechanically generated waves in clean water and with the highest concentration Γ_8. At CYGNSS cut-off wavenumber $k_c = 7.5$ rad/m indicated in the figure, we see a difference of the two values of MSS which is not significant but larger than the difference in cases of floating particles. A more quantitative picture is shown in Fig. 5(b), which shows the MSS averaged over the six sensors and computed at $k_c = 7.5$ rad/m. Comparing the clean-water result and the result with Γ_8, we see a reduction of MSS by $O(10\%)$. For wind-wave cases, Fig. 5(c)-(e) show the MSS at sensor 6 for different concentration levels (for which waves are excited). In these figures we see clear difference of MSS even at $k_c = 7.5$ rad/m. Quantitatively, with surfactant concentration levels Γ_2, Γ_3 and Γ_5, the MSS is reduced by 8%, 17% and 50% relative to the clean-water results for wind speeds of 4.29, 6.59, and 9.09 m/s, respectively. Considering the CYGNSS MSS anomaly which is $O(20\%)$ (in terms of the reduction from the Katzberg model results), it is clear that the presence of surfactants in wind seas is the most influential factor for this remote application.

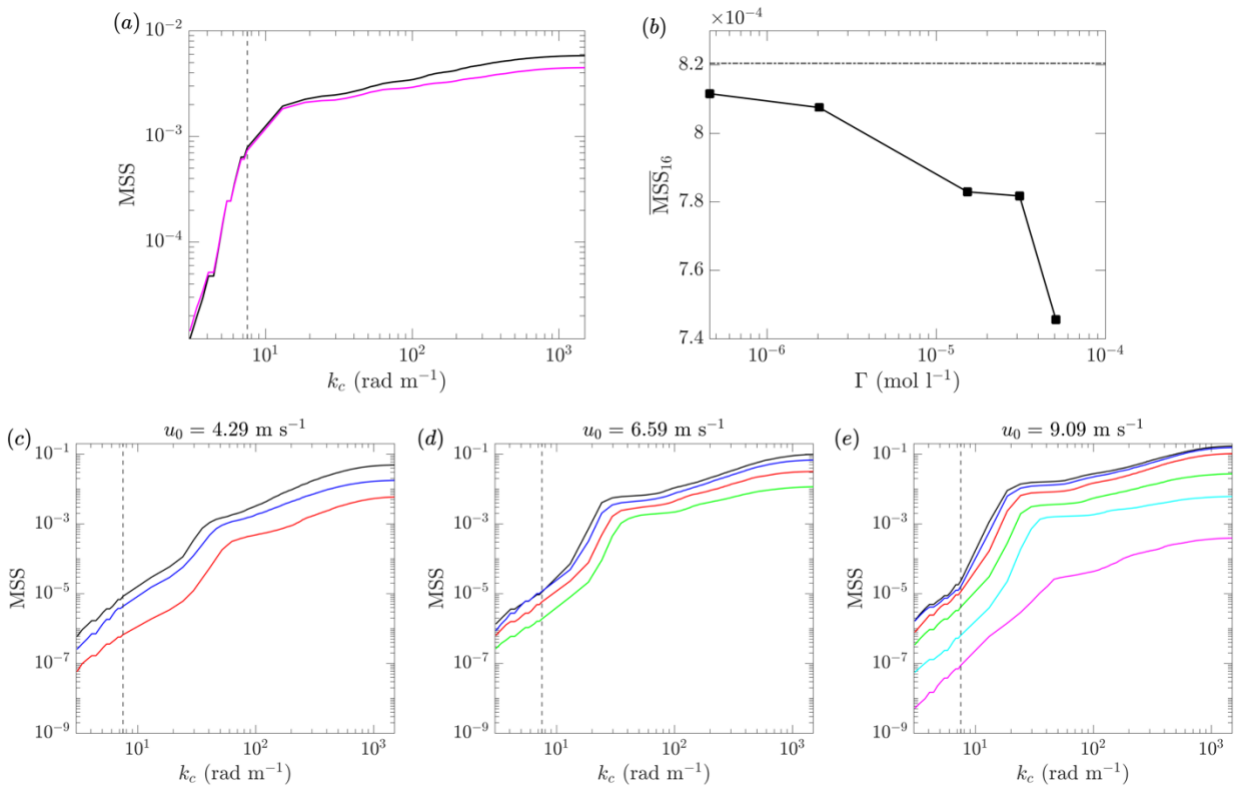

Fig. 5. (a) MSS as a function of cut-off wavenumber k_c for mechanically generated waves with surfactant concentrations Γ_0 (black line) and Γ_8 (magenta line); (b) MSS averaged over the six sensors and computed with $k_c = 7.5$ rad/m for different concentration levels Γ for mechanically generated waves, with result from Γ_0 marked (dash-dotted line); (c-e) MSS as a function of k_c at reference wind speeds of 4.29, 6.59, and 9.09 m/s, respectively, with surfactant concentrations Γ_0 (black line), Γ_1 (blue line), Γ_2 (red line) , Γ_3 (green line), Γ_4 (cyan line), and Γ_5 (magenta line). The locations of $k_c = 7.5$ rad/m are indicated by vertical dashed lines in (a) and (c-e).

References

Evans, M. C., C. S. Ruf (2021). Towards the Detection and Imaging of Ocean Microplastics with a Spaceborne Radar. IEEE Trans. Geosci. Remote Sens., doi: 10.1109/TGRS.2021.3081691.

Ruf, C. S., R. Atlas, P. S. Chang, *M. P. Clarizia*, J. L. Garrison, S. Gleason, S. J. Katzberg, Z. Jelenak, J. T. Johnson, S. J. Majumdar, A. O'Brien, D. J. Posselt, A. J. Ridley, R. J. Rose, V. U. Zavorotny (2016). New Ocean Winds Satellite Mission to Probe Hurricanes and Tropical Convection. Bull. Amer. Meteor. Soc., doi:10.1175/BAMS-D-14-00218.1.

van Sebille, C. Wilcox, L. Lebreton, N. Maximenko, B. D. Hardesty, J. A. van Franeker, M. Eriksen, D. Siegel, F. Galgani, K. L. Law (2015). A global inventory of small floating plastic debris" Environ. Res. Lett. doi:10.1088/1748-9326/10/12/124006.

Sun, Y., C. S. Ruf, T. Bakker, Y. Pan (2021), Effects of microplastics and surfactants on surface roughness of water waves, https://arxiv.org/abs/2111.07021

Lapham, G. S., D. R. Dowling, W. W. Schultz (1999). In situ force-balance tensiometry. *Experiments in Fluids* 27, 157-166.

Katzberg, S. J., O. Torres, G. Ganoe (2006). Calibration of reflected gps for tropical storm wind speed retrievals. *Geophysical Research Letters* 33 (18).

Wang, T., V. U. Zavorotny, J. Johnson, Y. Yi, C. Ruf, S. Gleason, D. McKague, P. Hwang, E. Rogers, S. Chen, Y. Pan, T. Bakker (2020). Improvement of CYGNSS level 1 calibration using modeling and measurements of ocean surface mean square slope. *IEEE International Geoscience and Remote Sensing Symposium,* pp. 5909-5912.